

Nonuniform Cooling of the Eclipsed Moon: A Listing of Thirty Prominent Anomalies

Abstract. *Infrared scanning during a total eclipse has revealed hundreds of hot spots, many identified with craters smaller than the detector resolution. Areal corrections show that some of these features may have the thermal properties of bare rock. Correlation of thermal response with albedo and radar reflectivity shows discrepancies. There is a concentration of hot spots in Mare Tranquillitatis.*

The temperature of the lunar surface falls markedly during a total eclipse (1). For example, the subsolar point, starting at about 400°K, cools to half that value during the penumbral phase. During totality, when heat is extracted from the subsurface, the surface cools more slowly, dropping another 20°K or so before sunlight again falls upon it. Such eclipse measurements, together with comparable dark-side measurements, imply that the surface is covered by material of low density and thermal conductivity. However, the surface does not cool uniformly, a number of ray craters and other areas (not well identified previously) having been observed to cool more slowly than their environs

(2, 3). We have developed a focal plane scanner for infrared (10 to 12 μ) and visible (0.45 μ) measurements on the illuminated lunar disk (3); with this device we scanned the moon in the infrared repeatedly during the total eclipse of 19 December 1964, with the 74-inch Kottamia telescope of the Helwan Observatory in Egypt, in order to survey the thermal anomalies on the lunar disk.

Preliminary results, reported recently (4), revealed the following: (i) As expected, thermal anomalies were found on the major ray craters. (ii) Hundreds of localized thermal anomalies, or "hot spots," were discovered, which were not distributed randomly over the surface. (iii) Some maria, or parts of other

maria, were found to be elevated in temperature compared to their surroundings. The data were recorded on magnetic tape for computer reduction and construction of isothermal contours. We have devised a system for producing, from the tapes, an infrared image of the moon on an oscilloscope. Figure 1, an image made from a scan program during totality, summarizes our results. For orientation purposes, the large anomaly near the bottom is Tycho and the one somewhat to the left of center is Copernicus.

The identification of the thermal anomalies, 400 of which have now been cataloged, shows that most (~ 90 percent) are craters which are visually bright in some respect at full moon (ray craters or craters with bright interiors or rims). The remaining are associated with "white areas" at full moon (for example, in Deslandres), which may have a very small crater (for example, Linné or Posidonius γ), or with rilles, such as Rima Hadley.

We attempted to order the most prominent anomalies from the chart recordings made during the experiment. For instance, from the third and last scan program made in totality, Dawes, Tycho, the white area in Deslandres, Guericke C, Dionysius, Messier A, Cauchy, and Diophantus gave the largest signal differences above their environs, in that order. However, the ordering of the thermal features by the signal differences showed wide discrepancies between the three scans made during totality, and it was soon apparent that this was due to the smallness of many features compared to the resolution element of the infrared detector (10" arc, or 1/100th of the lunar radius). The scan line positions were not identical on the lunar disk for the three scan programs, because of the rotation of the moon and change of its size in the focal plane. Therefore, features smaller than the resolution element would often be observed successively on two scan lines (which were separated by one resolution element), and the relative value of these two signals was very sensitive to exactly how the anomaly was intersected.

Therefore, for the purpose of presenting a meaningful ordering of the thermal anomalies, an areal correction has been applied to the signal differences. For simplicity we assumed in this report that the anomaly originated only from the crater and that the temperature was uniform therein. Correc-

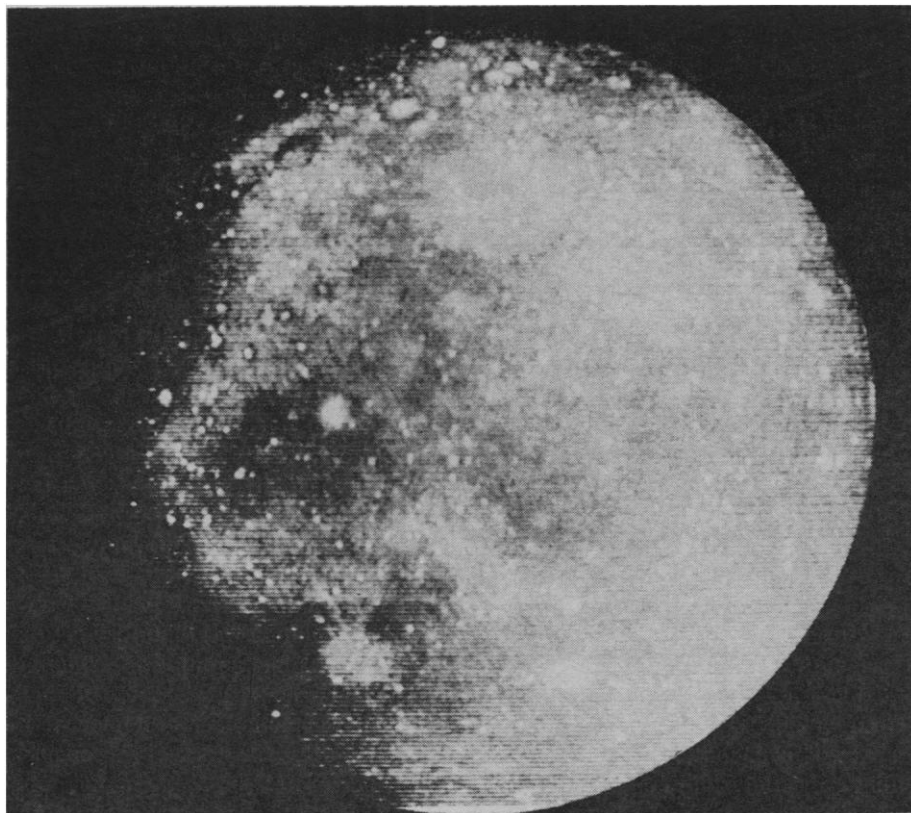


Fig. 1. A thermal image of the moon reconstructed from 200 line scans recorded during the total eclipse of 19 December 1964. As expected from previous work, the major ray craters cooled less rapidly than their environs. The image also reveals the presence of hundreds of "hot spots" (most of which are associated with small craters) and thermal enhancements in some or portions of the lunar seas. On the image, north is inclined 30° to the left of vertical.

tions were thus made that took into account the crater diameter, its projection onto the detector aperture, and the relative values of signal differences above the environs on successive scan lines (occasionally the signal was observed on only one scan line). For some large craters such as Tycho, where thermal variations were observed within the crater, we used a value averaged over the crater, rather than the peak value. No correction was made for the anomalous "white areas" or rilles, since it was not entirely clear over what area these features were anomalous. With this procedure, 83 anomalies with the largest signal differences were studied; after the corrections mentioned were made, the 30 largest anomalies were ranked as shown in Table 1. Of the 30 anomalies listed in the table, 6 are ray craters, 20 are white spots (craters with bright interiors), and 4 have bright rims. Also, of these 30 anomalies, 23 fall in the maria, 5 in the highlands, and 2 are uncertain (Cephus A falls on the rim of Cephus and Eudoxus A is in an area not easily identified as upland or maria). Seventeen of the white spots fall in maria.

There are some limitations in the correction described and the ranking procedure. For example, the ranking was done strictly on corrected signal differences above the environs: no normalizations were employed to take into account differences in initial signal before the eclipse began. Hence, features near the limb, starting at a lower temperature than those near the center, may be ranked somewhat lower than they should be. Also, only 83 features were studied; no doubt there are anomalies associated with very small craters which were not included because of the small apparent differences on the chart recordings, but which, if an areal correction were made, would have to be included in the ranking (the correction goes roughly as the inverse square of the crater diameter). Further, in examining the corrected signal differences for each feature from the three totality scans, in some cases one value was out of line with the other two and was not included. Actually, such discrepancies may be due to oversimplifications in the correction procedure; more refined methods are being considered. No doubt the best means for studying the small hot spots is by infrared scanning, during an eclipse, at an even higher resolution.

Sixty-three of the 83 anomalies studied are associated with craters of

Table 1. Ranking of 30 prominent thermal anomalies on the eclipsed moon. Crater diameters are thousandths of a lunar radius. For relative ranks, read down, not across; for example, Egede A ranks 16th.

Crater	Diameter	Crater	Diameter	Crater	Diameter
Mösting C	2.20	Guericke C	6.30	Cauchy	7.11
Piton B	2.82	Flamsteed B	5.50	Gambart C	7.01
Messier A	7.84	Taruntius H	4.86	Carlini D	5.34
Buch B	3.90	Jansen F	5.47	Eudoxus A	8.12
Jansen E	4.08	Marius A	9.30	Pico B	6.61
Torricelli B	4.00	Egede A	7.22	Cephus A	7.25
Draper C	4.48	Laplace A	5.00	Hesiodus B	5.90
Maraldi B	4.27	Nicollet	8.80	Janssen K	9.00
Moltke	3.70	Mösting A	7.50	Bode A	7.10
Plato M	4.81	Mason C	7.14	Carlini	6.54

known diameter; for these a plot was constructed (Fig. 2) of the corrected signal differences as a function of crater diameter. The points represent perhaps 5 percent of the anomalies discernible at our resolution, and since we have selected only the more prominent anomalies, they represent the upper boundary of a general distribution of a much larger number of anomalies. Figure 2 shows that larger signal differences are

observed on the smaller craters (although, of course, there are many small craters which are not thermally anomalous). The corrected signal differences were converted to temperatures and compared with Jaeger's theoretical model of the eclipse cooling for a homogeneous surface (5). For this model, a family of cooling curves is characterized by different values of a thermal parameter; in Fig. 2 values of

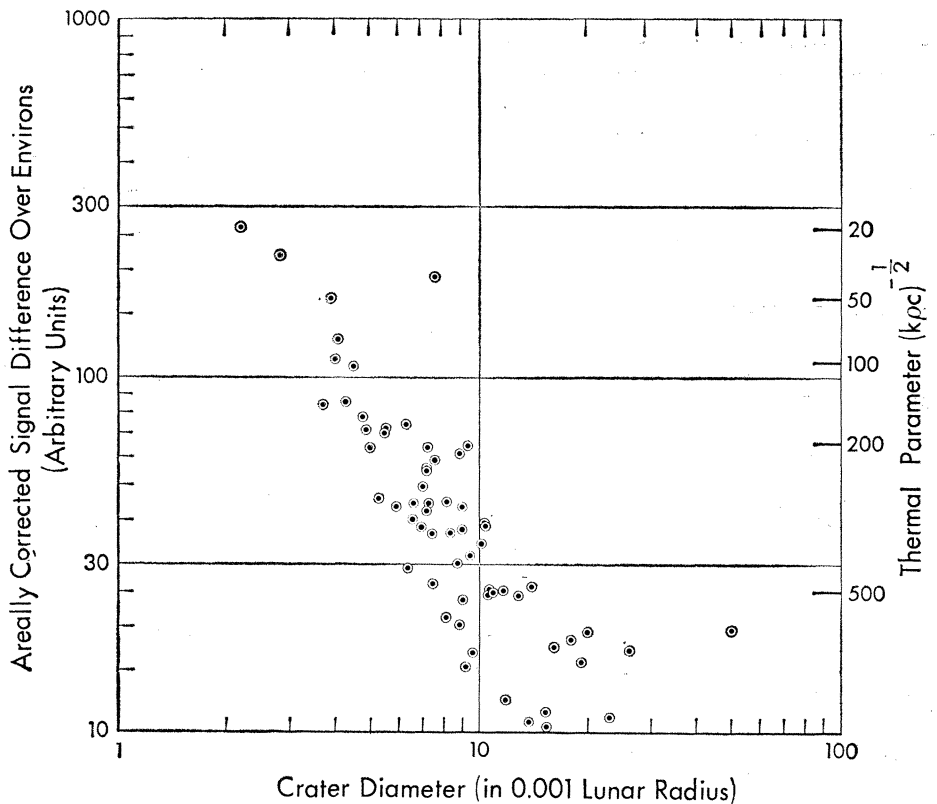


Fig. 2. Distribution of thermal anomalies versus crater diameters. Our resolution element corresponds to 0.01 of a lunar radius. The signal differences, when compared to the theoretical cooling of a homogeneous model of the lunar surface, correspond to the indicated values of the thermal parameter $(k\rho c)^{-1/2}$, where k is the thermal conductivity, ρ the density, and c the heat capacity. This parameter has a value of about 20 for rock, 100 for dry sand, and 1000 for powdered dust in a vacuum (in calories and centimeter-gram-second units).

this parameter are indicated for the corresponding signal differences. Mösting C, the most prominent anomaly on our list, has an indicated value for this parameter of ~ 20 , which is characteristic of bare rock. Therefore, this crater probably represents a young feature which has been exposed for a relatively short time to the erosional and blanketing processes which are responsible for the highly insulating properties of the older lunar surface.

The interpretation of these thermal features on the eclipsed moon is outside the scope of this report, but several puzzling aspects of the problem can be mentioned. First, although the hot spots are associated with bright features, conversely, there are bright features which are not thermally anomalous; thus there does not appear to be a direct relationship between visual brightness and the thermal response. For example, the ray craters Menelaus and Dionysius have the same brightness and appearance at full moon, but during the eclipse Menelaus was only 11°K warmer than its environs, whereas Dionysius was 44°K warmer. Further, the ray crater Euclides was only slightly warmer than its environs during totality, even though other craters similar in size and appearance gave large thermal responses. Second, the fact that ray craters show enhanced radar returns as well as anomalous eclipse cooling has been cited as showing that the surface of these features is denser or rougher, or both. However, a comparison of the radar reflectivity contours (6) with our infrared eclipse data shows there is no simple correlation between the measurements. For instance, enhanced radar returns are found on Eratosthenes and Posidonius, but these craters do not show anomalous eclipse cooling. Also, the radar contours for the ray craters Copernicus and Tycho are decidedly different from their isotherms during totality. It is interesting to note that the uplands give a higher radar return than the maria; the reverse is generally true for the infrared eclipse data. Since the two experiments do not measure the same parameters, it may not really be surprising that there is some lack of correspondence, and, in fact, the differences between them may be as interesting as the similarities. Finally, the nonrandom distribution of hot spots (there is a concentration in Mare Tranquillitatis) can be understood in terms of a random impact origin of the craters if the original surface in which

they were formed had local properties which in some way enhanced and prolonged the anomalous thermal behavior. On the other hand, this nonrandom distribution might not be surprising if the craters were formed by internal processes. In fact, internal processes may explain the anomalies observed on the "white areas," which give the appearance of being caused by a deposition of some material of higher albedo over areas large compared to their sources on the surface.

R. W. SHORTHILL
J. M. SAARI

Boeing Scientific Research
Laboratories, Seattle, Washington

References and Notes

1. W. M. Sinton, in *Physics and Astronomy of the Moon*, Z. Kopal, Ed. (Academic Press, New York, 1962), p. 407.
2. J. M. Saari and R. W. Shorthill, *Icarus* **2**, 15 (1963); B. C. Murray and R. L. Wildey, *Astrophys. J.* **139**, 734 (1964).
3. R. W. Shorthill and J. M. Saari, *Ann. N.Y. Acad. Sci.* **123**, 722 (1965).
4. J. M. Saari and R. W. Shorthill, *Nature* **205**, 964 (1965).
5. J. C. Jaeger, *Australian J. Phys.* **6**, 10 (1953).
6. T. W. Thompson, paper presented at URSI [International Scientific Radio Union] Meeting, Washington, D.C., 20-24 April 1965.
7. This research was sponsored in part by Air Force Cambridge Research Laboratories, Office of Aerospace Research, under contract 19(628)-4371. We thank Dr. A. H. Samaha, director, Dr. M. K. Aly, associate director, and the staff of the Helwan Observatory for observing time and assistance in carrying out the experiment. G. K. Bruce, E. S. Hedman, and T. K. Deaton assisted in collecting and reducing the data.

18 June 1965

Anomalous Dispersion Method: Its Power for Protein Structure Analysis

Abstract. The phases of x-ray reflection of a crystal can be measured, except for an ambiguity, if the crystal contains heavy atoms which scatter x-rays anomalously. Theoretical studies show that the method of resolving this ambiguity by choosing the phases closer to those of the heavy atoms has a good potentiality for solving complicated structures, in which the average heavy atom contribution to the intensity is as low as 10 percent.

The use of anomalous dispersion effects for resolving the phase ambiguity in the isomorphous replacement method was first pointed out by Bijvoet (1). The theory was tested and proved in a known structure, that of L-ephedrine hydrochloride, by Ramachandran and Raman (2). The method leads to two

ambiguous values for the phase, one of which will be closer to that of the heavy anomalous scatterers than the other. By choosing the phase closer to that of the heavy atoms as suggested (2), Raman (3) determined an unknown structure, that of L-lysine monohydrochloride dihydrate, using this technique with projection data. Since then, this method (which may be called the quasi-anomalous method) has been applied for two more structure analyses, that of Factor V 1a of Dale *et al.* (4) and of methyl melaleucate iodoacetate (5). The relevant data regarding these are given in Table 1, in which σ_1^2 is the mean fractional contribution to the intensity by the known anomalous scatterers and is equal to the ratio

$$\frac{\sum_{j=1}^P f_j^2}{\sum_{j=1}^N f_j^2}$$

where P represents the known atoms, N all the atoms, and f_j is the scattering factor of the atom j (6).

It has been shown by theory (7) that the fractional number of reflections n_{90° , for which the phase differs by less than 90° from that of the heavy atoms, is a function of σ_1^2 , which increases by an increment of σ_1^2 . The number of reflections also changes slightly depending on the number of heavy atoms in the unit cell. Thus, n_{90° is 94 percent when σ_1^2 is equal to 0.8, is as high as 82 percent even when σ_1^2 is 0.4, and is 62 percent when σ_1^2 is 0.1 (Table 2), with two heavy atoms in the unit cell. Therefore the quasi-anomalous method would work even for a value of σ_1^2 as low as 10 percent, which is much lower than the value of 26 percent, which is the lowest for which a structure analysis has yet been made (4). With the view of testing this, the quasi-anomalous method was applied to a hypothetical case containing 24 carbon and 22 oxygen atoms in the unit cell—in the same locations as in the structure of cellobiose (8), with two additional anomalously scattering atoms, each with a scattering power of half that of a chlorine atom ($\sigma_1^2 = 10$ percent). When the phase closer to the heavy atom was chosen, the Fourier synthesis (Fig. 1) was obtained for the c -projection. There are clear peaks of electron density at all the unknown atomic locations and very few false peaks.

In fact, the diagram can be improved with a weighting function W , whereby